NIKHEF

Mechanical behaviour of a closed collar model for an 11.5 T dipole magnet

W. van Emden, C. Daum, J. Geerinck

NIKHEF-H, P.O. Box 41882, 1009DB Amsterdam,
the Netherlands

A. den Ouden, H.H.J. ten Kate, D. ter Avest, S. Wessel

Applied Superconductivity Centre, University of Twente,
P.O. Box 217, 7500AE Enschede, the Netherlands

R. Dubbeldam

HOLEC Inc., P.O. Box 4050, 2980 GB Ridderkerk,
the Netherlands

Abstract: A 10 cm long model of an 11.5 T Nb_3Sn accelerator dipole magnet, which will be built in the Netherlands, with a closed ring shaped collar has been constructed. Measurements of the collar deformation and the prestress at the poles have been made. A comparison of these results is made with a structural analysis using the Finite Element Method (FEM) of the code ANSYS.

Mechanical behaviour of a closed collar model for an 11.5 T dipole magnet

W. van Emden, C. Daum, J. Geerinck
NIKHEF-H Amsterdam

A. den Ouden, H.H.J. ten Kate, D. ter Avest, S. Wessel
Applied Superconductivity Centre Enschede

R. Dubbeldam
HOLEC Ridderkerk

Abstract: A 10 cm long model of an 11.5 T Nb_3Sn accelerator dipole magnet, which will be built in the Netherlands, with a closed ring shaped collar has been constructed. Measurement of the collar deformation and the prestress at the poles have been made. A comparison of these results is made with a structural analysis using the Finite Element Method (FEM) of the code ANSYS.

1   Introduction

The 10 T NbTi twin-aperture dipole magnets have a horizontally split collar enclosing the coil packages of the two apertures in the CERN-LHC reference design [1,2]. For closing and locking of the collars around the coil packages at room temperature, an additional prestress has to be applied. This has the disadvantage that the applied prestress is higher than the prestress required for the collaring. This may cause yield of the material around the locking pins or keys resulting in loss of prestress after cooldown and excitation.

In this paper we present a new collar design in which the prestress in the coil is achieved by shrink-fitting a closed ring shaped collar around the coil package of each aperture. A 10 cm length model with a dummy coil has been produced for the determination of manufacturing tolerances, the mechanical properties of materials, and the mechanical behaviour of this concept. Comparison is made with extensive FEM calculations using the ANSYS code [3] performed on a fully impregnated 11.5 T twin-aperture dipole with Nb_3Sn cable. We have included the effects of friction in these computations.

1

2 General layout

The current density of Nb3Sn wires and cables [4] produced with the ECN powder technique [5] promises a target field for an LHC dipole magnet of 11.5 T at 4.2 K, but modifications of
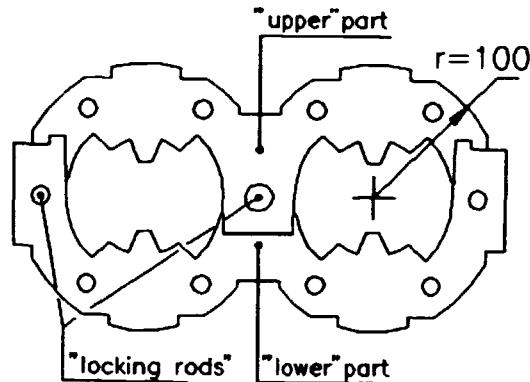

Fig. 1. Horizontally split collar.

the collar and coil design are essential to reach this goal. In comparison with the reference design [1,2] two major changes are made. First, a closed ring shaped collar is introduced which eliminates the need for the holes for the locking rods in the traditional design of Fig. 1. This results in an increase of the bending stiffness of the collar. Also, the outer coil diameter can be increased from 120.2 to 129.4 mm. This provides space for adding superconductor in radial direction. The second major modification is a reoptimization of the cable dimensions and coil layout. The increase in diameter of the coils results in an increase in diameter of the collars and of the iron return yoke. To keep the overall diameter of the magnet within the original limits the outer aluminium shrink cylinder is replaced by a stainless steel cylinder. The main characteristics are listed in Table 1.

Table 1 Main characteristics of the LHC dipole magnet		
magnetic field	11.5	T
maximum field in inner layer	11.8	T
maximum field in outer layer	9.6	T
inner coil diameter	50.0	mm
outer coil diameter	129.4	mm
maximum Lorentz force in x-direction	6.5	MN/m
maximum Lorentz force in y-direction	-1.6	MN/m
maximum Lorentz force on coil head	0.9	MN
operating current	17.7	kA
cable dimensions inner layer	1.98/2.47 x 21.7	mm^2
critical current inner layer @ 12 T	20.6	kA
cable dimensions outer layer	1.55/1.93 x 17.4	mm^2
critical current outer layer @ 10 T	20.0	kA

"UPPER" PART

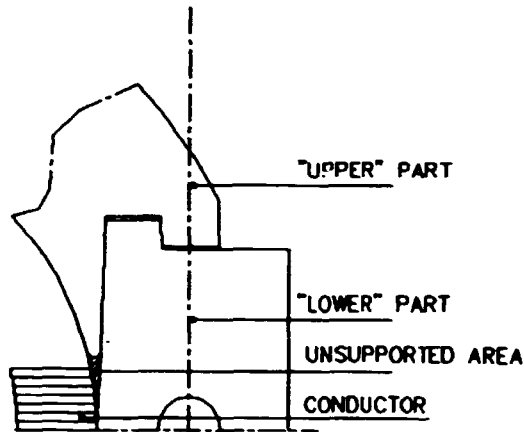"LOWER" PART

UNSUPPORTED AREA

CONDUCTOR

Fig. 2. Detail at the locking rod of the horizontally split collar.

3   The split collar concept

In the LHC design, the twin-aperture magnet will be built with a horizontally split collar. This concept has been used in all superconducting accelerator magnets (Tevatron, HERA) up to now. In the Tevatron and HERA magnets the stress limit of coil materials and collars are not yet reached and a slight overstress during collaring is not harmful. However, for LHC magnets the stress levels are close to yield limits of materials.

The horizontally split twin-aperture LHC dipoles introduce another complication. The collars are split into two non-symmetric parts, as shown in Fig. 1. A large press is needed which has to provide the compressive force for the two apertures simultaneously. At room temperature, the required prestress is obtained by the external compressive force, which is taken over by the pins or keys after release of the external press and locking of the collars. Plastic yield may occur in the collars around the pins or keys. The resulting stress distribution is inhomogeneous due to the split. The collars do not support the coil everywhere in the region of the split as shown in Fig. 2. Locally, the coil is supported by only every second collar. After cooldown, when the prestress reaches its maximum, large stresses between collars and rods or keys can locally introduce additional plastic yield which reduces the prestress on the coils.

In some LHC dipole design variants and in one MTA1 model magnet built and tested in 1991 separated coil/collar systems for each aperture have been used [6].

4   The closed collar concept

To avoid the problems with a horizontally split collar as mentioned above we have studied the application of a closed collar around each aperture. Two advantages are obvious. First, the stiffness of the collar is increased significantly. Second, the collared coils for each aperture can be finished and tested separately. This enables a magnetic match between different coil packages before the enclosure in the common yoke.

This concept has been studied in view of the use of Nb_3Sn superconductor for the design of a twin-aperture dipole magnet which should reach a field of 11.5 T. This superconductor is brittle after reaction and the critical current degrades under longitudinal strain. The strain should be limited to less than 0.3%.

The coils are made of a Rutherford cable of Nb3Sn conductor in a copper matrix, and are produced with the "wind and react" technique. The coils are fully impregnated after reaction. The impregnated coil packages consist of Nb3Sn cables, copper spacers and stainless steel poles and have a cylindrical shape. The collars should now be circular inside. Each aperture has its own collar as shown in Fig.3. Adjacent collars have a flat outer interface. All collars are in contact with the coil over the entire circumference. The stress distribution in the collar is not interrupted by pins or keys.
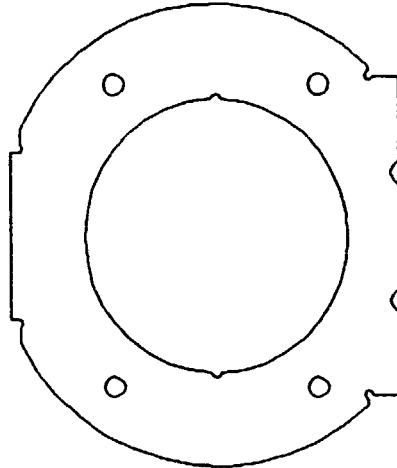

Fig. 3. The closed ring shaped collar.

Collaring is achieved by heating the collars to 225 °C which provides a annular slot of 0.36 mm between the hot collar and the coil which is at room temperature. The required prestress of the coils is obtained by the shrink fit after cooldown of the collars to room temperature.

5   The closed collar concept and Nb3Sn coils

The pole inserts are made of stainless steel for obtaining the required prestress at 4.2 K by the differential contraction of collars, coils and pole inserts. The prestress of the coil at the poles is determined by the Young's modulus of the various materials. The Young's modulus of the Nb3Sn cable is not well known. Fig. 4 shows the prestress and the coil stress after excitation over the expected range of the Young's modulus of the coil. The Young's moudulus is taken to be isotropic and not orthotropic as in [2]. During the design the tolerable upper stress limit on the coil has been set at 150 N/mm^2 after excitation [7]. On the other hand contact between coils and poles has to be assured under all circumstances. The lower prestress limit appears to be 15 N/mm^2. These limits generate a tolerable spread of this Young's modulus between 18000 and 24000 N/mm^2 which is reasonable compared with measurements on impregnated stacks of cables. In this design a Young's modulus of 20000 N/mm^2 has been used. The copper matrix of the Nb3Sn strands has a very small yield stress ($\approx$ 35 N/mm^2) after reaction of the Nb3Sn filaments at 700 °C during about 48 hours. This requires a hardening of the coils after impregnation and before collaring by pressing them to their final dimensions to avoid uncontrolled plastic deformation.
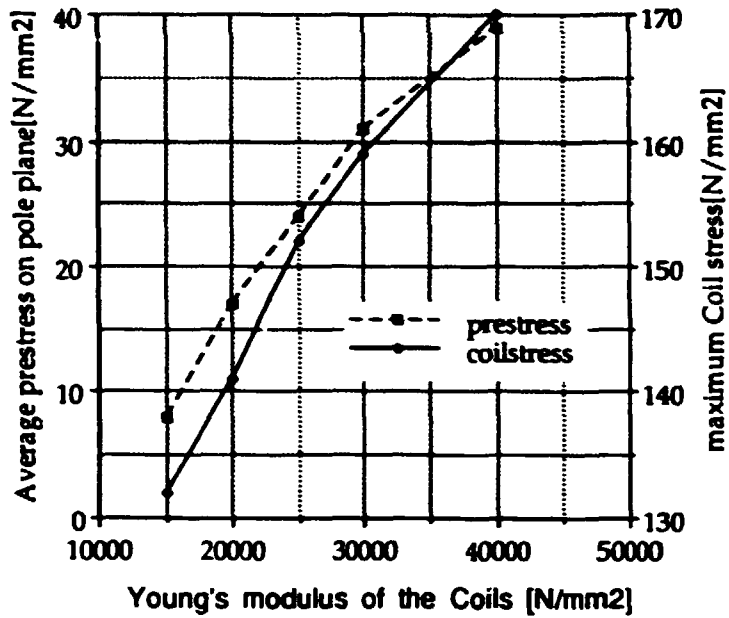
Fig.4. The calculated relation between the average prestress on the pole plane and the Young's modulus of the coils.

6 Finite element calculations

The CERN-LHC design [2] describes the complete structural FEM analysis of the twin-aperture LHC dipole magnet consisting of coils, collars, return yoke and outer shrink cylinder. The calculations presented here are based on this structure but now for closed collars, Nb3Sn cables in the new conductor layout [8], and a stainless steel outer shrink cylinder. The cross section of this magnet is shown in Fig. 5.
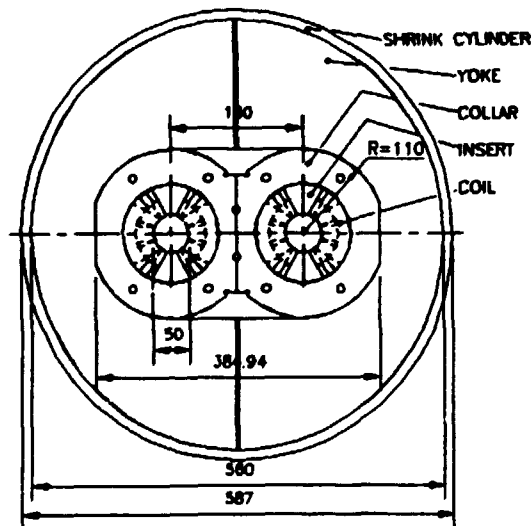

Fig. 5. Cross section of the dipole magnet.

5

Table 2						
Summary of the structural analysis without friction, $\mu = 0$, of the dipole magnet of Fig. 6						
Material of the outer cylinder						stainless st.
Dimensions of the inclined gap of the iron yoke (mm)						0.465/0.337
Load case		Collaring	Clamping	Outer Cyl.	Cooldown	Excitation
Input						
$T_{reference}$	K	328	328	328	328	328
T_{insert}	K	478	478	478	189	189
T_{collar}	K	328	328	328	39	39
T_{coil}	K	453	453	453	164	164
T_{spacer}	K	466	466	466	177	177
T_{yoke}	K	328	328	328	39	39
$T_{cylinder}$	K	328	328	243	-46	-46
Field	T					11.5
Outer cyl.						
σ_{eq}	N/mm^2			130	217	219
$F_{cyl,x}$	N			1291	2033	2073
$F_{cyl,y}$	N			1296	2043	2082
Yoke						
ΣF_m	N		0	0	1749	268
$\Sigma F_{i,normal}$	N		0	892	503	1109
$\Sigma F_{i,slide}$	N		0	0	0	0
σ_{eq}	N/mm^2		20	192	121	180
Δx_a	mm		0.0826	-0.177	-0.465	-0.465
Δy_a	mm		0.00047	-0.066	-0.766	-0.797
Δx_b	mm		0.0823	-0.154	-0.377	-0.337
Δy_b	mm		0.00047	-0.051	-0.417	-0.440
Δx_c	mm		0.0832	-0.094	-0.724	-0.645
Δx_d	mm		0.0801	-0.099	-0.915	-0.846
Collar						
$\Sigma F_{c,normal}$	N		100	1292	283	1803
$\Sigma F_{c,slide}$	N		0	0	0	0
σ_{eq}	N/mm^2	103	92	124	161	223
Δy_e	mm	0.033	0.043	0.117	-0.406	-0.493
Coils						
ΣF_{normal}	N	1393	1438	1941	2724	823
ΣF_{slide}	N	0	0	0	0	0
σ_{eq}	N/mm^2	63	61	108	116	138
σ_0	N/mm^2	34.8	35.9	48.5	68.1	20.6
Δx_f	mm	0.125	0.0941	-0.08	-0.547	-0.452
Δx_g	mm	-0.008	-0.01	-0.01	-0.123	-0.133
Insert						
σ_{eq}	N/mm^2	92	121	448	285	70

6

7 Calculations without friction

The structural analysis is made in the same way as in Ref. [2] using a similar mesh and ignoring friction. In Table 2 a summary is listed of the displacements (Δx, Δy) at the points "a" - "g", and the forces (F) in a quadrant of the cross section of the dipole as shown in Fig.6 at various steps of the load cycles of the structure. Also equivalent stresses (σ_{eq}, maximum von Mises Stress) in various components and the average prestress (σ_0) on the coil at the pole are given. Initial conditions of the components are controlled by their temperature (T) in the analysis.
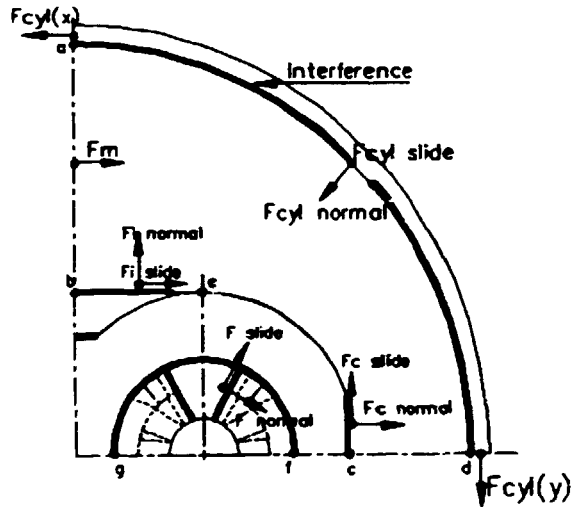

Fig. 6. Quadrant of the coil cross section with definition of the forces and the positions of points "a" - "g" used in the FEM calculations.

8 Calculations with friction

A structural analysis which includes the effects of friction requires a redefinition of the mechanical properties of the interface elements between adjacent surfaces which may slide relative to each other to simulate the effect of a copper-beryllium sliding foil. The interference regions are shown in Fig. 6. Sliding of an interface element is defined by a normal force F_n and a friction coefficient μ. No motion occurs, if the sliding force F_s tangential to the surface has a value $F_s < \mu F_n$.

A proper description of friction requires a correct modelling of the normal stiffness K_n and the tangential stiffness K_s to avoid numerical problems [9]. The stiffnesses are described reasonably by $K_n = E A / H$ and $K_s = G A / L$, where E is Young's modulus, G the shear modulus, A the sliding area, H the normal length and L the tangential length as shown in Fig. 7.

If $F_s \geq \mu F_n$, sliding occurs and energy is lost. This behaviour is non-conservative (load path dependent). The total load should be applied successively in separate load steps from assembly to full excitation of the magnet. The interface is characterized by two states: "sliding"
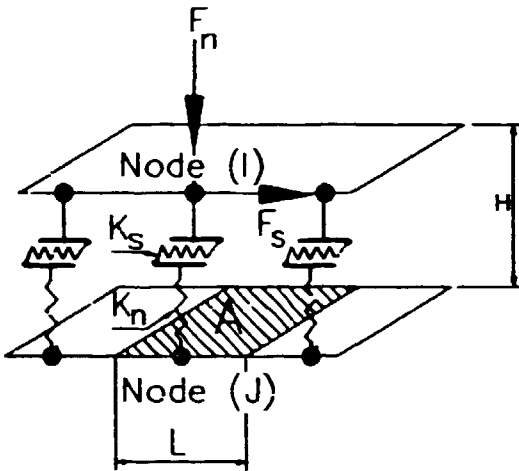
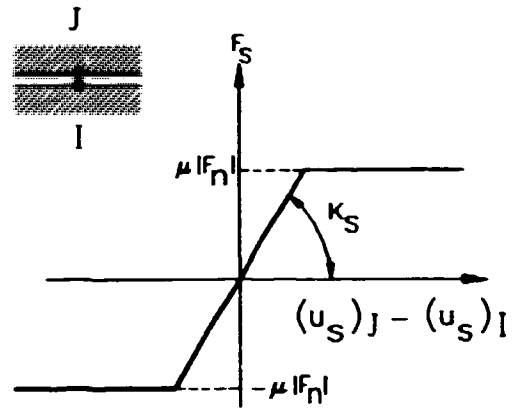**Fig. 7.** *Model for the description of friction.* **Fig. 8.** *Illustration of quantities used to describe the "sliding" and "non-sliding" state.*

or "non-sliding". The two states are illustrated in Fig. 8. In the case of "non-sliding" ($F_s < \mu F_n$), the relation between F_s and $(u_s)_J - (u_s)_I$, the relative tangential displacement of J and I, is given by the line with slope K_s. In the "sliding" case, the relation is indicated by the horizontal lines which is identical to the case of no friction. Convergence occurs, when the status is unchanged from the previous state.

For the calculations, the load history from assembly to full excitation is divided in 13 load steps. Each of these has to converge before going to the next step. The 13 load steps are scheduled as follows:

step nr.	load path
1	collaring
2	clamping
3	outer cylinder applied
4 - 8	cooldown
9 - 13	excitation.

9 The coefficient of static friction

The friction coefficient for the used pair of materials has not been measured. From a metallurgical point of view the insertion of CuBe sheet at all sliding planes is expected to lower the friction coefficients effectively and it prevents probably slip stick motion.

Experiments on the measurement of the friction coefficient μ show a strong dependence on the measuring conditions [10]. Generally, on unlubricated surfaces μ appears to be high. A value of 0.4 seems to be reasonable for this case [11]. To investigate the problem arising from friction in detail, calculations with $\mu = 0.2, 0.3, 0.4$ and 0.6 have been made.

8

Table 3						
Summary of the structural analysis with friction, $\mu = 0.4$, of the dipole magnet of Fig. 6						
Material of the outer cylinder						stainless st.
Dimensions of the inclined gap of the iron yoke (mm)						0.465/0.337
Load case		Collaring	Clamping	Outer Cyl.	Cooldown	Excitation
Input						
$T_{reference}$	K	328	328	328	328	328
T_{insert}	K	478	478	478	189	189
T_{collar}	K	328	328	328	39	39
T_{coil}	K	453	453	453	164	164
T_{spacer}	K	466	466	466	177	177
T_{yoke}	K	328	328	328	39	39
$T_{cylinder}$	K	328	328	243	-46	-46
Field	T				11.5	
Outer cyl.						
σ_{eq}	N/mm²			183	207	215
$F_{cyl,x}$	N			1312	1514	1682
$F_{cyl,y}$	N			2370	2578	2810
Yoke						
ΣF_m	N		0	0	1146	0
$\Sigma F_{i,normal}$	N		0	671	282	762
$\Sigma F_{i,slide}$	N		0	244	36	90
σ_{eq}	N/mm²		20	114	121	166
Δx_a	mm		0.112	-0.0794	-0.455	-0.448
Δy_a	mm		0.0004	-0.0534	-0.756	-0.786
Δx_b	mm		0.111	-0.0648	-0.337	-0.334
Δy_b	mm		0.0004	-0.0463	-0.414	-0.434
Δx_c	mm		0.113	-0.0247	-0.724	-0.647
Δx_d	mm		0.109	-0.0297	-0.91	-0.848
Collar						
$\Sigma F_{c,normal}$	N	0	100	1068	331	1772
$\Sigma F_{c,slide}$	N	0	8	78	25	292
σ_{eq}	N/mm²	111	110	123	202	176
Δy_e	mm	0.0267	0.0385	0.0864	-0.394	-0.477
Coils						
ΣF_{normal}	N	1490	1562	2119	2901	1068
ΣF_{slide}	N	142	120	177	459	407
σ_{eq}	N/mm²	67	64	79	142	153
σ_0	N/mm²	37.3	39.0	52.9	72.5	26.6
Δx_f	mm	0.141	0.1242	-0.00917	-0.546	-0.453
Δx_g	mm	-0.0077	-0.0099	-0.011	-0.124	-0.136
Insert						
σ_{eq}	N/mm²	113	116	329	386	97

10 The results of the analysis including friction

The computations are performed on a transverse cross section with a longitudinal thickness of 1 mm. All resulting forces refer therefore to an imaginary magnet with a length of 1mm. The layout of the components in the cross section is shown in Fig. 6. The results for $\mu = 0.4$ are shown in Table 3.

After collaring the insert does not slide along the pole plane which results in a 7 % higher prestress (σ_0) than in the case of no friction. During the load case of "clamping" the different parts do not slide relative to each other and friction has hardly any effect in this particular load case. During the load case of "application of the outer cylinder" the iron yoke and the stainless steel shrink cylinder can slide relative to each other because of the open gap of the yoke. In addition to large normal forces between the two parts large friction forces will develop along the plane of the yoke and the outer cylinder: $F_{cyl,slide} = F_{cyl,x} - F_{cyl,y} = 1048$ N. Due to this large friction force and the sliding force on the plane "b-e" in Fig. 6, the iron yoke will move less inward. The bending of the yoke will also decrease resulting in a reduction of the normal force on the "b-e" plane. Hence, this sliding force will introduce a shear stress in the copper-beryllium sliding foil which can be calculated as follows:

$$\tau = F_{cyl,slide} / A = 2.4 \text{ N/mm}^2.$$

At cooldown the inclined gap between the two yoke parts is closed, but the mating force Fm on the vertical plane will be 34 % less than in the frictionless case. After excitation the mating force between the yoke parts is insufficient which results in a reopening of the gap up to 34 μm, i.e. $\Sigma F_m = 0$ at full excitation (see Table 3).

Friction causes an increase in average contact stress between the poles and the outer coils. Large friction forces along the pole plane introduce an inward bending of the coils at the pole causing a loss of contact between coil and pole at the inner radius. The highest field is present at this radius which makes the coil very sensitive to quenching due to coil motion. Table 4 shows the normal and sliding force along the pole plane for $\mu = 0$ and $\mu = 0.4$ at the positions "A" to "I" in Fig. 9.

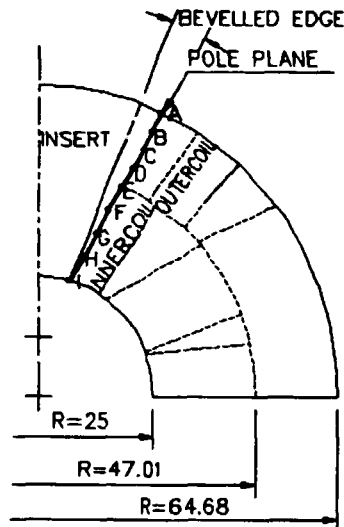| Table 4 Normal and sliding force along the pole plane at the positions "A" - "I" in Fig. 9				
Part	Position	F_{normal} ($\mu = 0$)	F_{normal} ($\mu = 0.4$)	F_{slide} ($\mu = 0.4$)
		N	N	N
Outer coil	A	0	97	39
	B	0	197	7
	C	113	224	89
	D	202	247	97
	E	172	150	55
Inner coil	F	95	89	32
	G	107	58	14
	H	93	6	2
	I	41	0	0

Fig. 9. Pole plane and position of points "A" - "I" used in the FEM calculations. Bevelling of the edge of the insert along the line "A" - "I" determined by its displacement at "A".

Table 5 shows the average inner and outer contact stress on the pole plane for $\mu = 0$ and $\mu = 0.4$.

The results for coefficient of friction $\mu = 0, 0.2, 0.3, 0.4$ and 0.6 at maximum excitation are shown in table 6, where $\Sigma F_m = 0$ for $\mu = 0.3, 0.4$ and 0.6.

Fig. 10 shows the impact of friction on the total structure after excitation. It shows the differential stresses and displacements between $\mu = 0.4$ and $\mu = 0$.

Table 5 Contact stress on the pole plane			
Part	σ_0 ($\mu = 0$)	σ_0 ($\mu = 0.4$)	
Outer coil	22.7	47.5	N/mm^2
Inner coil	19.2	10.4	N/mm^2

11 Optimization of the mechanical structure

Calculations with friction show an opening up of the gap of the two yoke parts and a less homogeneous distribution of the prestress on the pole plane than for the case without friction. Therefore, the gap between the two yoke parts has been changed to 0.407 mm at "a" and 0.29 mm at "b" in Fig. 6. With this improved geometry the gap remains closed after excitation to 11.5 T, and the mating force is $\Sigma F_m = 284$ N for $\mu = 0.4$.

To obtain a better distribution of the prestress calculations have been made with a bevelled edge of the insert. Fig. 9 shows bevelling of the edge of the insert for 0.05, 0.075 and 0.1 mm at point "A". Fig 11 shows the prestress along the pole plane for the various angles of bevelling. These results give also an impression of the sensitivity for dimensional tolerances.

Table 6

Summary of the structural analysis for various values of friction of the dipole magnet of Fig. 6

Material of the outer cylinder						stainless st.
Dimensions of the inclined gap of the iron yoke (mm)						0.465/0.337
Load case		Excitation	Excitation	Excitation	Excitation	Excitation
Friction coefficient		$\mu = 0$	$\mu = 0.2$	$\mu = 0.3$	$\mu = 0.4$	$\mu = 0.6$
Input						
$T_{reference}$	K	328	328	328	328	328
T_{insert}	K	189	189	189	189	189
T_{collar}	K	39	39	39	39	39
T_{coil}	K	164	164	164	164	164
T_{spacer}	K	177	177	177	177	177
T_{yoke}	K	39	39	39	39	39
$T_{cylinder}$	K	-46	-46	-46	-46	-46
Field	T	11.5	11.5	11.5	11.5	11.5
Outer cyl.						
σ_{eq}	N/mm^2	219	207	212	215	254
$F_{cyl,x}$	N	2073	1819	1752	1682	1554
$F_{cyl,y}$	N	2082	2417	2607	2810	3255
Yoke						
ΣF_m	N	268	78	0	0	0
$\Sigma F_{i,normal}$	N	1109	924	850	762	606
$\Sigma F_{i,slide}$	N	0	43	69	90	167
σ_{eq}	N/mm^2	180	178	175	166	166
Δx_a	mm	-0.465	-0.458	-0.452	-0.448	-0.435
Δy_a	mm	-0.797	-0.791	-0.789	-0.786	-0.778
Δx_b	mm	-0.337	-0.337	-0.335	-0.334	-0.329
Δy_b	mm	-0.440	-0.437	-0.436	-0.434	-0.428
Δx_c	mm	-0.645	-0.649	-0.646	-0.647	-0.648
Δx_d	mm	-0.846	-0.849	-0.846	-0.848	-0.848
Collar						
$\Sigma F_{c,normal}$	N	1803	1784	1825	1772	1720
$\Sigma F_{c,slide}$	N	0	264	285	292	295
σ_{eq}	N/mm^2	223	214	203	176	168
Δy_e	mm	-0.493	-0.484	-0.483	-0.477	-0.469
Coils						
ΣF_{normal}	N	823	897	1031	1068	995
ΣF_{slide}	N	0	179	281	407	539
σ_{eq}	N/mm^2	138	145	150	153	166
σ_0	N/mm^2	20.6	22.4	25.8	26.6	24.9
Δx_f	mm	-0.452	-0.455	-0.452	-0.453	-0.469
Δx_g	mm	-0.133	-0.135	-0.135	-0.136	-0.138
Insert						
σ_{eq}	N/mm^2	70	105	94	97	178

Fig. 10. The difference in displacements and stress distribution at full excitation for μ = 0.4 and μ = 0.

12 Assembly of the dummy model of the closed collar system

A 10 cm long dummy model has been manufactured for measuring the deformations of the collars and the prestress in the pole planes at room temperature and at 77 K for comparison with and judging of the accuracy of the calculations.

The dummy model consists of 33 collar plates, each 3 mm thick, aligned by four stainless steel centre pins. The geometry of the coils is simulated by two brass pieces. Although a material with a Young's modulus similar to that of an impregnated coil would have been preferable it has been decided to use brass elements for meeting manufacturing tolerances. The separate pole inserts in which space is left for introducing stress transducers are made of stainless steel. The coil pieces and pole inserts are manufactured by electric discharge milling. The inserts, transducers and coil pieces are tightly wrapped with a 0.4 mm x 25 mm CuBe foil providing in a smooth cylindric coil package. The aluminium collar plates have a thickness of 3 mm and are produced by milling for reducing costs. Although it seems difficult to meet the absolute accuracy the differences between the plates are well within tolerances. Fig. 12 shows the assembly of the model.

The assembly of the model is performed by heating the stacked collar plates up to 225 °C for creating a sufficiently large annular slot between the inside diameter of the collar stack and the outside diameter of the dummy coils. The coils are lowered into the stacked collar plates and reach the final position in 5 s after which it was still possible to pull the coil out of the collars. Shrinking of the collars around the coils has been repeated many times. This experience has demonstrated that this procedure is well suited for a 1 m long magnet. It has not yet been decided whether the stacked collars will be heated up, or alternatively the finished coil will be cooled down to 77 K to create the required mounting space. Cooling of the coils eliminates the danger of reduction of the yield strength of the aluminium which might occur when the collars are heated up for a period of several hours. However, that procedure needs a more complicated setup.
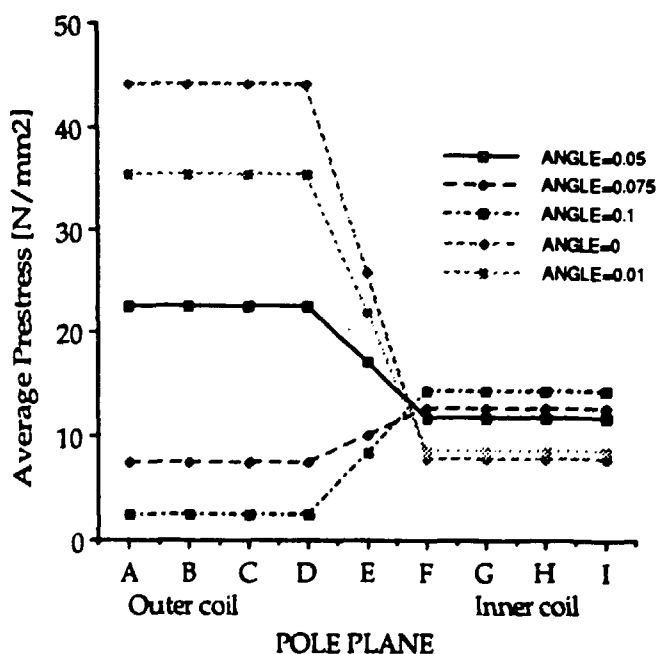

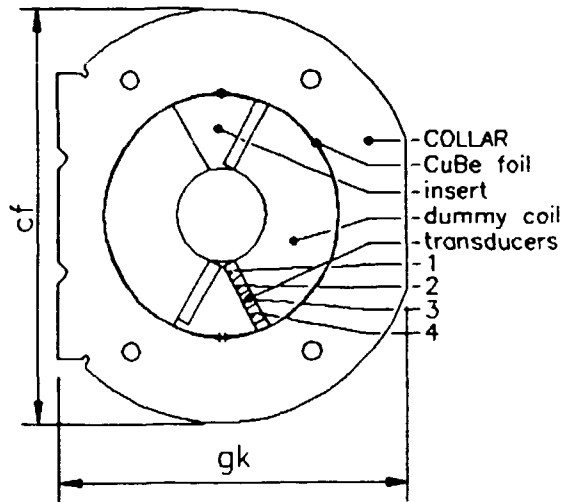Fig. 11. Average prestress along pole plane for various angles of bevelling.

Fig. 12. Dummy model of closed collar system.

13 Measurements on the dummy model

The normal stress at the pole plane is measured with beam type strain gauge transducers (Fig. 13). To enable the registration of radial stress gradients four independent transducers are mounted adjacently along the pole plane. Their operation relies on bending of the beam by an applied normal stress which is assumed to be hydrostatic. This condition is met if the transfer material is soft compared to the beams which are made of stainless steel. Ideally this results in a linear relation between the applied stress and the measured change in resistance of the strain gauge.

The strain gauge transducers have been calibrated in a test setup which simulated the measuring conditions in the model. Fig. 14a shows a typical calibration curve in the case a glass-epoxy transfer block is used between the press and the transducers. The upper and lower curves correspond to beam models of different size. No measurable shift in the individual curves occurs if the relative order in position of the transducers is changed indicating good reproducibility. The manufacturing tolerances are assumed to be responsible for the difference in slope of a few percent and the behaviour at low stress. The estimated inaccuracy of these calibrations amounts to 5 %. This experience shows that this transducer layout is well suited to register the normal pole stress component in the 1 m magnet.
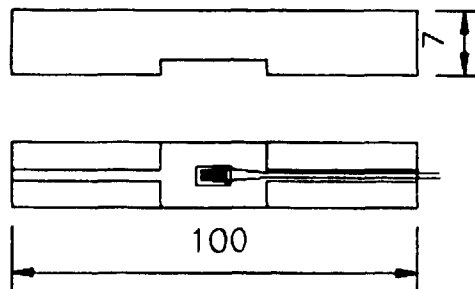

Fig. 13. The beam type strain gauge transducer.

The same calibrations are performed using a brass transfer block as used in the model. In this case the condition of hydrostatic stress transfer is hardly met and deviation from the linear behaviour has to be expected. This is demonstrated in Fig. 14b. Beside these changes rather large differences in individual response occur and the transducers are not anymore interchangeable. The reproducibility is poor and the inaccuracy is increased to 15 % during one and the same calibration run. The model measurements should therefore be interpreted accordingly.
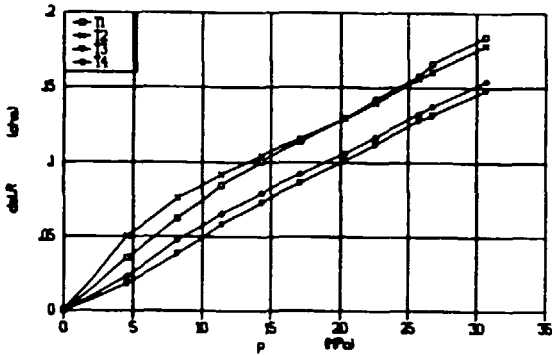

Fig. 14a. Typical calibration curves of four parallel transducers loaded by a glass-epoxy stress transfer block.
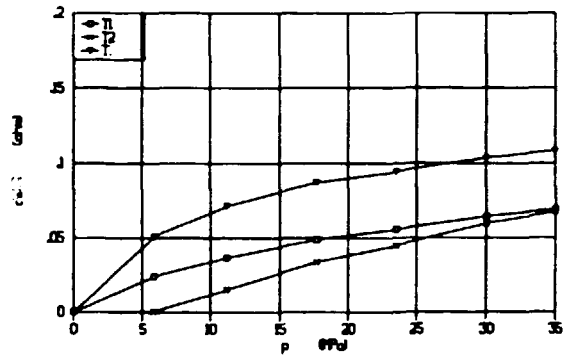
Fig. 14b. Calibration curves of three out of four parallel transducers loaded by a brass transfer block.

After collaring, the deformations of two major dimensions, "gk" and "cf", were measured (see Fig. 12). These were determined before and after collaring with an absolute error of 0.02 mm. The relative error in the measured prestress is 15 % as discussed above. The results are listed in Table 7 and compared with the calculations. The deformations appear to be systematically lower than the predictions and therefore a lower prestress would be expected. Under the restrictions mentioned above the registered stresses confirm the expected levels at 300 K and 77 K.

Table 7
Measured and calculated values of prestress and deformations

Temp.		Stress (N/mm^2)				Deformation (μm)	
		Transducer				Δ"gk"	Δ"cf"
		1	2	3	4		
300K	measured	62	51	49	67	80	120
	calculated	54	54	54	54	120	160
77 K	measured	87	95	85	96		
	calculated	80	80	80	80		

At this point it is useful to investigate the sensitivity of the measured quantities to dimensional tolerances. Fig. 15 and Fig. 16 show the calculated relation between the deviation from the nominal dimensions of the inner collar diameter on the prestress at the poles and the deformation of the collar, respectively, after collaring. A deviation of 0.02 mm which is the manufacturing tolerance results in a large variation of the prestress, whereas the deformation is

of the same order as the deviation itself. The influence of a small gap between inserts and coils on the pole plane on the same measurable quantities is shown in Figs. 17 and 18, respectively. Both dimensional tolerances may be responsible for the rather large differences between measured and calculated deformations. Although it is difficult to measure the dimensions with the required accuracy at every assembly stage, this experience indicates the importance of regular measurements of main dimensions during manufacturing and assembly of the coil and collar system.
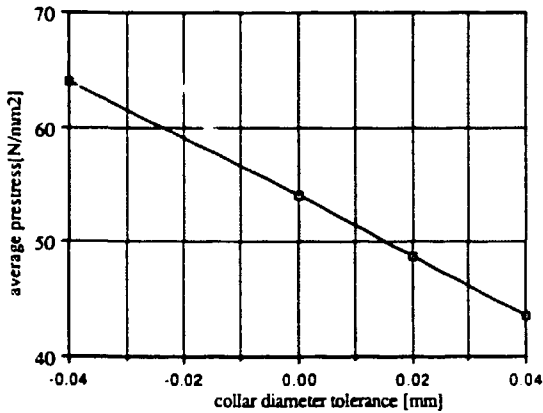

Fig. 15. The average prestress as function of the tolerance on the diameter of the collar.
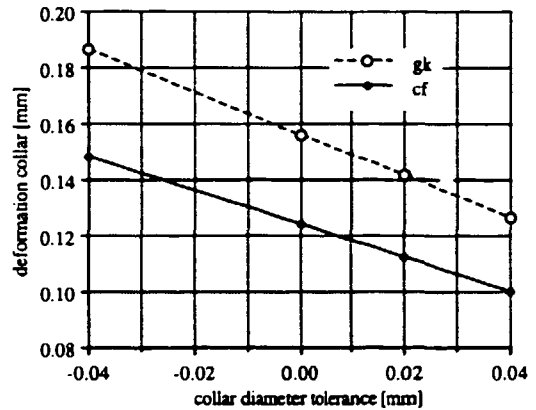
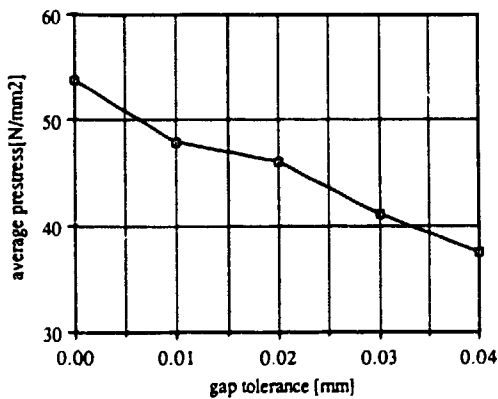Fig. 16. The deformation of the collar as function of the tolerance on the diameter of the collar.

Fig. 17. The average prestress versus as of the tolerance on the gap between the contact plane of the insert and the dummy coil.
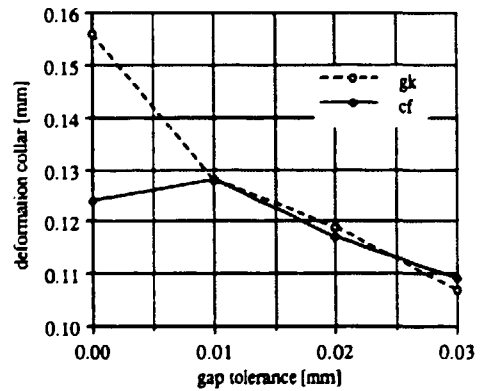
Fig. 18. The deformation of the collar function as function of the tolerance on the gap between the contact plane of the insert and the dummy coil.

17

14 Conclusions

The finite element analysis of an 11.5 T Nb₃Sn LHC dipole magnet equipped with closed collars around each aperture has shown the applicability of this collar system. The shrinking process of the collars around the coils has been repeated many times with the short dummy model and is expected to cause no problems in the assembly of a 1 m magnet.

A systematic study of stresses and deformations inside the structure could be used to define the manufacturing tolerances of the various components. Studies of the effects of friction on the structural behaviour have been performed. For reasonable values of the friction coefficient between 0 and 0.6, two major problems arise. First, the gap between the iron yoke parts does not remain closed at full excitation. Second, contact loss between coil and pole inserts at the pole plane occurs. The main source of these effects is the friction force between the yoke and the shrink cylinder. Proper lubrication might reduce these effects significantly. These calculations show the potential vulnerability of the hybrid support structure.

From measurements on a short dummy model of the coil system it is conclude that measured and calculated deformations and stresses agree within limits imposed by manufacturing tolerances. The beam type strain gauge transducers are suitable for monitoring transverse stresses in the system provided a proper calibration procedure precedes their final mounting.

References

1. The Large Hadron Collider in the LEP tunnel, Eds. G. Brianti and K. Hübner, CERN 87-05, 27 may 1987.
2. D. Leroy, R. Perin, D. Perini and A. Yamamoto, "Structural analysis of the LHC 10 T twin-aperture dipole", CERN SPS/89-32 (EMA), LHC Note 103, and Proceedings of the 11th International Conference on Magnet Technology, MT11, Tsukuba, Japan, August 28 - September 1, 1989, p. 159.
3. ANSYS, Trade mark of SWANSON Analysis Inc., Houston, Texas, USA.
4. H.H.J. ten Kate, B. ten Haken, S. Wessel, J.A. Eikelboom, E.M. Hornsveld, "Critical current measurements of prototype cables for the CERN LHC up to 50 kA and between 7 and 13 Tesla using a superconducting transformer circuit", Proceedings of the 11th International Conference on Magnet Technology, MT11, Tsukuba, Japan, August 28 - September 1, 1989, p. 60.
5. E.M. Hornsveld, J.D. Elen, C.A.M. van Beijnen, P. Hoogendam, "Development of ECN-type Niobium Tin wire towards smaller filament size", Adv. Cryog. Eng. 34, 493, 1987.
6. H. Hirabayashi, A. Yamamoto, S. Kawabata, G. Brianti, D. Leroy, R. Perin, "Design study of a superconducting dipole model magnet for the LHC", Proceedings of ASC90, Snowmass, Colorado, September 24-28, 1990.
   M. Bona, D. Leroy, R. Perin, P. Rohmig, B. Szeless, W. Thomi, "Design and fabrication variants and results of LHC twin-aperture models", presented at the 12th International Conference on Magnet Technology, MT12, Leningrad, June 23 - 28, 1991.
7. H.H.J. ten Kate, S. Wessel, H. Boschman, L.J.M. van der Klundert, "The reduction of the critical current in Nb3Sn cables under transverse forces", presented at the 12th International Conference on Magnet Technology, MT12, Leningrad, June 23 - 28, 1991.
8. D. ter Avest, H.H.J. ten Kate, L.J.M. van der Klundert, "Optimizing the conductor dimensions for a 10 - 13 T superconducting dipole magnet", Proceedings of ASC90, Snowmass Colorado, September 24-28, 1990, paper LCP31.
   D. Ter Avest, "Properties of the Superconductor in Accelerator Dipole Magnets", Thesis, University of Twente, Netherlands, June 20, 1991.
9. SWANSON Analysis Systems, Inc., "Structural Nonlinearities Seminar" DN-S201:44, October 9, 1989.

10. E. Rabinowicz, "The Determination of the Compatibility of Metals through Static Friction Tests", MIT, Cambridge, Mass., USA.
11. R.L. Tobler, "A Review of Antifriction M aterials and Design for Cryogenic Environments", National Bureau of Standards, Boulder, Colorado, USA.